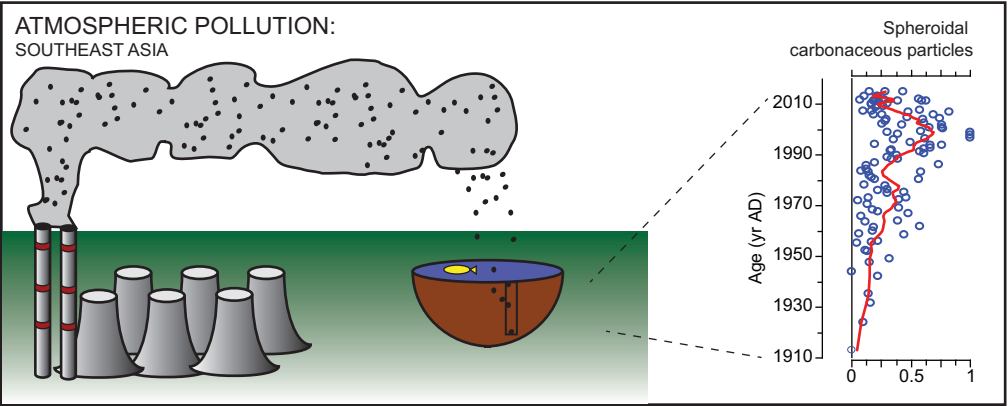
ATMOSPHERIC POLLUTION:
SOUTHEAST ASIA
Spheroidal
carbonaceous particles
Age (yr AD)
2010
1990
1970
1950
1930
1910
0
0.5
1

Historical atmospheric pollution trends in Southeast Asia inferred from lake sediment records

Engels S[1,2*], Fong LSRZ[3], Chen Q[3], Leng MJ[1,4], McGowan S[1,5], Idris M[6], Rose NL[7], Shafiq M[6], Taylor D[3], Yang H[7]

Affiliations
[1] Centre for Environmental Geochemistry, School of Geography, University of Nottingham, Nottingham, NG7 2RD, UK
[2] School of Geography, Birkbeck University of London, Malet Street, London, WC1E 7HX, UK
[3] Department of Geography, National University of Singapore, Singapore, 117570, Singapore
[4] NERC Isotope Geosciences Facilities, British Geological Survey, Nottingham, NG12 5GG, UK
[5] School of Environmental and Geographical Sciences, University of Nottingham-Malaysia Campus, Jalan Broga, 43500 Semenyih, Selangor Darul Ehsan, Malaysia
[6] Tasik Chini Research Centre, Faculty of Science and Technology, Universiti Kebangsaan Malaysia, 43600, Malaysia
[7] Environmental Change Research Centre, Department of Geography, University College London, London, WC1E 6BT, UK
[*] author for correspondence; s.engels@bbk.ac.uk

Abstract

Fossil fuel combustion leads to increased levels of air pollution, which negatively affects human health as well as the environment. Documented data for Southeast Asia (SEA) show a strong increase in fossil fuel consumption since 1980, but information on coal and oil combustion before 1980 is not widely available. Spheroidal carbonaceous particles (SCPs) and heavy metals, such as mercury (Hg), are emitted as by-products of fossil fuel combustion and may accumulate in sediments following atmospheric fallout. Here we use sediment SCP and Hg records from several freshwater lentic ecosystems in SEA (Malaysia, Philippines, Singapore) to reconstruct long-term, region-wide variations in levels of these two key atmospheric pollution indicators. The age-depth models of Philippine sediment cores do not reach back far enough to date first SCP presence, but single SCP occurrences are first observed between 1925 and 1950 for a Malaysian site. Increasing SCP flux is observed at our sites from 1960 onward, although individual sites show minor differences in trends. SCP fluxes show a general decline after 2000 at each of our study sites. While the records show broadly similar temporal trends across SEA, absolute SCP fluxes differ between sites, with a record from Malaysia showing SCP fluxes that are two orders of magnitude lower than records from the Philippines. Similar trends in records from China and Japan represent the emergence of atmospheric pollution as a broadly-based inter-region environmental problem during the 20th century. Hg fluxes were relatively stable from the second half of the 20th century onward. As catchment soils are also contaminated with atmospheric Hg, future soil erosion can be expected to lead to enhanced Hg flux into surface waters.

‘Capsule’ – Lake sediment records from Southeast Asia provide first data on historical trends in fossil-fuel derived atmospheric pollution

Keywords: fossil fuel combustion; emission trends; fly ash particles; mercury; Southeast Asia

Highlights

- First data on historical atmospheric pollution trends in Southeast Asia
- Increase in SCP flux from 1960 onward indicates increased atmospheric pollution
- Recent decrease in SCP fluxes probably due to air pollution control
- Mercury fluxes are relatively high and might reflect local sources of pollution

Introduction

Asia has undergone strong economic growth over the last few decades leading to a doubling in regional energy consumption between 1980 and 2003 (Richter et al., 2005; Ohara et al., 2007), with a continuous growth of energy consumption being observed since 2003 (Kurokawa et al., 2013; EANET, 2015). Fossil fuel combustion emits atmospheric pollutants, particularly SO_2, NO_x, CO, non-methane volatile organic compounds, organic carbon, black carbon and trace metals. Although pollutant emissions, particularly from the burning of coal, have been declining in Europe and North America over the last two decades, this has not been the case for much of Asia (Amann et al., 2013; Klimont et al., 2013; Kurokawa et al., 2013). While emissions of SO_2 and particulate matter ($PM_{2.5}$) decreased by 12-15% in East Asia between 2005 and 2010, emissions of NO_x and non-methane volatile organic compounds increased by 15-25% (Wang et al., 2014). Electricity demand in Southeast Asia (SEA), one of the world's fastest developing regions, is projected to be 83% higher in 2035 than in 2011 (International Energy Agency, 2013), with coal providing much of this increased energy demand (Lai et al., 2016).

Increased atmospheric pollution has major implications for society and the environment. An estimated 6.5 million deaths globally each year are attributed to poor air quality (International Energy Agency, 2016; World Health Organization Press, 2016). Koplitz et al. (2017) suggest that the current estimate of around 20,000 ($11.4–28.4 \times 10^3$) excess deaths per year due to emissions from burning coal in SEA will increase to around 70,000 ($40.1–126.7 \times 10^3$) by 2030. Perhaps contrary to common perception (Lai et al., 2016), around 9000 of these excess deaths as a result of increased coal use in SEA are anticipated to occur in China; rising coal emissions in SEA could thus become an increasingly transboundary pollution issue (Koplitz et al., 2017).

Atmospheric greenhouse gas concentrations resulting from fossil fuel combustion are one of the key drivers of anthropogenic climate change (IPCC, 2014), and aerosols (particularly atmospheric black carbon) can significantly influence global radiative forcings (Jacobson, 2001; Streets et al., 2004). Fine aerosol particles can further influence regional climate via surface dimming (Ramanathan et al., 2005; Lau et al., 2006); Fu et al., 2017). Atmospherically deposited pollution places further pressure on anthropogenically impacted wetlands and lowland lakes in SEA, with existing impacts including eutrophication, intensified aquaculture, water abstraction, dam construction, biomass burning, as well as catchment disturbances such as agriculture (e.g. oil palm and other plantations), urbanisation and mining activities (Sharip et al., 2014). Those aquatic ecosystems that have not been severely degraded yield valuable services, such as food and water for local populations and the provision of livelihood opportunities such as eco-tourism (Shuhaimi-Othman et al., 2007; Stockholm International Water Institute, 2009; Sharip and Jusoh, 2010). These services may be difficult to

replace. Moreover, human impacted aquatic ecosystems are likely to have significantly reduced biodiversity value (Kopf et al., 2015). Unfortunately, information on the current status of many of these ecosystems, and on the rates and directions of change in environmental conditions over recent decades, is generally lacking. In addition, detailed inventories of anthropogenic energy sources and emissions for Asia only span the last few decades (Kato and Akimoto, 1992; Akimoto 2003; Streets et al., 2003; Kurokawa et al., 2013) and their number is comparatively low (Ohara et al., 2007; Rose 2015).

Natural archives such as lake sediments have the potential to provide essential information on spatio-temporal variations in fossil fuel consumption in SEA, as spheroidal carbonaceous particles (SCPs), by-products of high-temperature industrial fossil fuel combustion, can be stored in these sediment records following atmospheric deposition, thus tracking changing influx with time (Rose 2015). SCPs are fine carbonaceous aerosols, typically 2–50 µm across, formed from the incomplete high-temperature combustion of fossil fuels such as oil and coal (Rose et al., 1994; Rose 2001; Chirinos et al., 2006). SCPs can be transported for thousands of kilometres through the atmosphere under favourable meteorological conditions (Rose et al., 1998; Yang et al., 2001; Inoue et al., 2014), and have been found in remote places such as the Falkland Islands and Antarctica, far removed from the nearest sources (Rose et al., 2012). SCPs are a component of the "black carbon continuum" (Rose, 2008; 2015), but whereas other components of black carbon can be the result of domestic emissions, road transport emissions, or biomass burning (e.g. Kurokawa et al., 2013), SCPs are only formed during high-temperature industrial fossil fuel combustion. As they have no natural sources, SCPs encountered in lake sediment records can be used as indicators of atmospheric deposition from industrial sources (Rose, 2001), especially as they are not susceptible to post-depositional alteration, movement in the sediment column (except by bioturbation), or degradation (Rose et al., 2003). Analysis of SCPs stored in sediments provides a means to reconstruct trends in emissions from the combustion of fossil fuels over time-periods that extend beyond the beginning of documentary and instrumental evidence, which commenced only in the second half of the 20th century and in some regions even more recently (Rose, 2001). Spatial patterns in SCP distribution have been shown to be closely linked to other pollutants, such as sulphur and polycyclic aromatic hydrocarbons (Rose and Juggins 1994; Rose et al., 1998; Barst et al., 2017). A global collation of SCP records includes a disproportionately large number of records from Western Europe and none from SEA (Rose, 2015).

Anthropogenic emissions of Hg date back to pre-industrial times, but global Hg emission rates have tripled over the last 150 years, mainly due to increased coal burning (Hylander and Meil, 2003; Engstrom et al., 2014; Horowitz et al., 2014; Yang et al., 2016). Aside from industrial sources,

there are many additional anthropogenic sources of atmospheric Hg emission, including waste incineration, sulphide ore processing, cement kilns and the production of various metals (Hylander and Meil, 2003). Another important potential source of atmospheric Hg is artisanal and small-scale gold mining (Mason and Pirrone 2009, Cordy et al., 2010). Hg is among the most toxic elements and poses serious threats to both human health and aquatic ecosystems due to its tendency to bioaccumulate and biomagnify through the food chain (Azimi and Moghaddam, 2013; Rice et al., 2014; Okelsrud et al., 2016). Mercury contamination in waterways, sediments and fishes in SEA are already threatening frigate birds as well as other species in the area depending on marine resources, including humans (Mott et al., 2017). With an atmospheric residence time of up to two years (Schroeder and Munthe, 1998), Hg can be released from the atmosphere through both wet and dry deposition. Hg can subsequently be stored in lake and wetland sediments, thereby providing the basis for reconstructions of past variations in pollution loads (e.g. Bindler et al., 2001; Fitzgerald et al., 2005; Yang et al., 2010; Shotyk et al., 2017).

Little information on past levels of industry-derived air pollution in SEA is available, especially for the period pre-dating 1980 (US Energy Information; www.eia.gov). This is despite the growing concerns of the effects of local and regional pollution in SEA (Koplitz et al., 2016). This paper addresses this information gap in long-term variations in air pollution deposition in SEA and uses sedimentary evidence as a basis for reconstructing changes in atmospheric pollution in SEA covering the period from the start of industrial fuel consumption to the present, including the time interval before 1980 where data on atmospheric pollution levels are otherwise scarce.

Materials and methods

Sites and sampling

Using logistical criteria such as site-accessibility and geographical spread, we selected sites from three countries in SEA in order to develop a regional reconstruction of atmospheric deposition pollution history: (1) sediment cores were obtained from three lakes in the Philippines (Yambo, Mohicap, Sampaloc) from the Seven Crater Lakes, a tight cluster of maar crater lakes located near San Pablo City, Laguna Province, on the island of Luzon (Fig. 1). The lakes are presumed to have formed through an explosive phreatic eruption from Mount Banahaw-San Cristobal (Brillo, 2016). The lakes are all moderately deep (>25 m water depth) and have surface areas ranging from 0.23 to 1.04 km^2 (Supplementary Table 1) (Aquino, 1983; Laguna Lake Development Authority, 2008). Lakes in the cluster are currently used for aquaculture across a range of intensities; those selected for this study range from relatively pristine (low level of aquaculture; Yambo) to heavily impacted (intensive aquaculture; Sampaloc). (2) Tasik Chini, a flood pulse wetland ecosystem in the state of Pahang,

Peninsular Malaysia, consists of 12 shallow, interconnected lake basins (Shuhaimi-Othman et al., 2007). The lake is under strong ecological pressure due to a range of anthropogenic activities in the area, including deforestation for rubber and oil palm plantations, mining, and artificial damming of the lake (Sharip and Jusoh, 2010). (3) There are no natural freshwater ecosystems with long sediment records available for study in Singapore. Instead, we sampled a reservoir (SR)[1], located in the largely forested Central Catchment of Singapore. Construction of SR began in 1970 with damming of the valley upstream of an existing reservoir (Public Utilities Board Website; http://www.pub.gov.sg).

Fieldwork was carried out in 2015 (Malaysia) and 2016 (the Philippines, Singapore). For each of our five selected sites we recovered a sediment core from the deepest part of the basin using a UWITEC gravity corer with an inner diameter of 86 mm. As the recovered sediments were highly organic and unconsolidated, core penetration varied between 72-104 cm. All cores preserved the sediment-water interface, and were subsampled in contiguous 1-cm-thick samples in the field.

Radiometric dating

Radiometric dates were obtained for the sediment cores from the Philippines and Malaysia by measuring ^{210}Pb, ^{226}Ra, ^{137}Cs and ^{241}Am using gamma spectrometry; the SR record was not radiometrically dated, although the lowermost part of the sediment core recovered post-dates the onset of reservoir construction (1970). Radiometric dating used freeze-dried sediment samples analysed in ORTEC HPGe GWL series well-type coaxial low background intrinsic germanium detectors at University College London. ^{210}Pb was determined via its gamma emissions at 46.5 keV, and ^{226}Ra by the 295 keV and 352 keV gamma rays emitted by its daughter isotope ^{214}Pb following three weeks of storage in containers (sealed with rubber stops to prevent loss of ^{222}Rn (Pittauerova et al., 2011)) to allow radioactive equilibration (Appleby et al., 1986). ^{137}Cs and ^{241}Am were measured by their emissions at 662 and 59.5 keV respectively (Appleby et al., 1986). A constant rate of supply (CRS) model was applied to each sediment core to create an age-depth model (Appleby, 2001). The CRS model assumes a constant rate of unsupported ^{210}Pb supply to the sediment (^{210}Pb derived from atmospheric fallout is unsupported ^{210}Pb), and is one of the most widely used methods for calculating ages based on ^{210}Pb activity (Appleby, 2001).

SCP analysis

[1] The reservoir is anonymized in line with a request from the Public Utilities Board (Singapore) who kindly granted access to the site

The SCP concentration of selected subsamples from all five study sites was determined following the protocol by Rose (1994). Dried sediment subsamples were digested with acids in order to remove organic, siliceous and carbonate sediment fractions. A known volume of processed subsample was then transferred to a coverslip and mounted on a glass microscope slide using Naphrax. SCPs were enumerated using a light microscope and expressed in concentration (number per gram of dry matter (gDM^{-1})). For the sites that were radiometrically dated, SCP concentrations were converted to flux (n cm^{-2} yr^{-1}) to take into account the variability in sediment accumulation rates (Rose et al., 1998). The detection limit for the technique is typically less than 100 gDM^{-1} (Rose, 1994), and concentrations presented here have an accuracy of c. ±30 gDM^{-1} for Tasik Chini and c. ±50-100 gDM^{-1} for the other records. Rose (1994; 2008) provides more details on the SCP preparation protocol and criteria for identification.

Mercury analysis

We measured Hg concentrations in the sediment cores from Sampaloc and Yambo (Philippines) using cold vapour-atomic fluorescence spectrometry (CV-AFS). Samples were digested with 8 mL aqua regia at 100 °C on a hotplate for 2 h in rigorously acid-leached 50 mL polypropylene digestion tubes, along with standard reference materials and sample blanks. The digested solutions (samples, standards and blanks) were subsequently analysed for Hg using CV-AFS following reduction with $SnCl_2$ (Yang et al., 2016). The standard reference material used here (GBW07305; stream sediment) has a certified Hg value of 100 ± 10 ng g^{-1}; our measured mean value was 103.8 ng g^{-1},with a relative standard deviation (RSD) of 3.1 ng g^{-1} (n=5).

Regional climate and atmospheric modelling

The monsoonal climate of SEA results in large intra-annual variations in the extent of the air-shed (the area from which a parcel of air, and suspended pollutants, is likely to be sourced) for each of the study sites. This is because seasonal changes in the monsoonal system result in differences in wind direction (Fig. 1) as well as in marked differences in wet and dry periods in most of the region (Supplementary Table 2). Peninsular Malaysia and Singapore are affected by two major monsoon systems, the southwest monsoon (late May-September; Supplementary Table 2) and the northeast monsoon (November-March), which brings high amounts of precipitation. During the transitional months, the equatorial trough lies over Malaysia and winds are generally light and variable. In the Philippines, the summer southwest monsoon brings relatively high amounts of precipitation to most of the archipelago during May-October. The northeast winter monsoon is generally associated with lower quantities of precipitation (Supplementary Table 2). The Philippines are also bisected by a

major tropical storm (typhoon) track, generally running east to west, with most major typhoons occurring between June and December (Kubota and Chan, 2009).

We analysed potential sources of atmospheric pollution for each of our sites by producing backward trajectories (72 h) of air masses for the Seven Crater Lake region (the Philippines), Tasik Chini (Peninsular Malaysia) and SR (Singapore) following Nagafuchi et al. (2009). The trajectories were plotted using the Hybrid Single-Particle Lagrangian Integrated Trajectory model (HYSPLIT) (Stein et al., 2015; Ready, http://www.ready.noaa.gov) using a weekly sampling resolution for five selected months (May 2016, August 2016, October 2016, November 2016, January 2017) that together represent the different modes of the monsoonal climate in SEA (Supplementary Table 2). The backward trajectory simulations started with air masses at 500 m above the modelled ground levels at starting point; trajectories were calculated based on meteorological data from the Global Data Assimilation System (NOAA, https://www.ready.noaa.gov/gdas1.php).

Results

Radiometric dating

The unsupported ^{210}Pb profiles show non-monotonic features in the Mohicap, Sampaloc and Tasik Chini records (Supplementary Table 3), confirming the suitability of the CRS model over the alternative, Constant Initial Concentration (CIC) model (Robbins, 1978). Activities of ^{137}Cs and ^{241}Am in these three records are too low to validate ^{210}Pb-based evidence for dating. While the Yambo ^{210}Pb profile shows a more regular pattern, small departures from an exponential decline also indicate the use of a CRS dating model for this core. A peak in ^{137}Cs activity at 39.5 cm depth in the Yambo record reflects the 1963 maximum in atmospheric ^{137}Cs fallout resulting from the testing of nuclear weapons. While ^{137}Cs can be mobile in natural environments, it is unlikely that the peak position would have changed. Therefore, the ^{137}Cs peak at 39.5 cm depth is used to correct the CRS ^{210}Pb chronology, which initially placed 1963 at 28.5 cm depth. The offset in the ^{210}Pb profile for the Yambo record might be the result of catchment-specific changes in sedimentation processes (such as changes in catchment erosion/inputs or sediment focussing) that might have changed the input of supported ^{210}Pb.

The resulting core chronologies (Fig. 2) suggest relatively high sedimentation rates at Mohicap, with an increase in rate of sedimentation between 1940 and 1970, followed by a uniform rate of 0.21 g cm^{-2} yr^{-1}. The Sampaloc record shows an increase in sedimentation rate around 1995, whereas the Yambo record shows relatively stable rates throughout. Rates of sedimentation are most variable in the Tasik Chini record, where step-wise increases can be seen around 1945 and 2000, with considerable variations during the last decade.

SCP records

Concentrations of SCPs in the three records from the Philippines and the record from Malaysia show similar trends, with first occurrences being observed in samples taken from the lower part of each core, followed by increasing concentrations in samples from higher in the sequence (Fig. 3). All records show decreasing concentrations in the uppermost part of the core. The concentrations differ from core to core, with maximum values reaching c. 40,000 SCPs gDM^{-1} at Sampaloc, but only c. 300 SCPs gDM^{-1} at Tasik Chini. The SR record shows continuous presence of SCPs from the onset of the core, with initial concentrations of SCPs of c. 800 SCPs gDM^{-1} around 70 cm core depth, subsequently increasing to maximum concentrations of c. 6000 SCPs gDM^{-1} at 45 cm core depth and with concentrations fluctuating between 2000-6000 SCPs gDM^{-1} in the upper part of the record.

First occurrences of SCPs often reflect early developments in the industrial combustion of coal and oil, and following two earlier samples with single occurrences of SCPs (Fig. 3) the Tasik Chini SCP flux record dates the onset of continuous presence of SCPs in sediment samples to c. 1950 (Fig. 4). The age-depth models of the cores from the Philippines do not reach back far enough to date first occurrences, and hence the SCP flux profiles are truncated. The Sampaloc record indicates that SCPs are encountered earlier than at Tasik Chini, with SCPs in the oldest sediment sample dated to c. 1925. The four radiometrically dated records all show increased SCP fluxes around 1960, although fluxes at Tasik Chini are much lower (10 cm^{-2} yr^{-1}) than the values observed at the Philippine sites (1000 cm^{-2} yr^{-1}). Three of the four records show a second step-change increase in SCP flux around 1990, with all records showing maximum flux at around 2000. All four records subsequently show decreasing flux to the present.

Mercury

Hg concentrations range between 30 and 150 ng g^{-1} in the Sampaloc and Yambo records (Fig. 5). In the core from Sampaloc, maximum concentrations of 90-150 ng g^{-1} are reached between 30 and 55 cm depth. Hg concentrations were initially low in Yambo (30-40 ng g^{-1} below 70 cm depth in the core), followed by relatively stable concentrations of 50-90 ng g^{-1} for the upper part of the record. When converted to flux, Hg in Sampaloc is around 40 µg m^{-2} yr^{-1} for most of the sequence, with an increase to values over 80 µg m^{-2} yr^{-1} between 1990 and 2005. The Yambo record initially shows a Hg flux of 60-90 µg m^{-2} yr^{-1} prior to 1965, after which it shows a relatively stable flux of c. 110 µg m^{-2} yr^{-1}.

Atmospheric modelling

Atmospheric modelling (Fig. 1) indicates seasonal differences in the air masses reaching our study sites throughout the year. The winter monsoon (November-April; Supplementary Table 2) delivers air masses from mainly the east-northeast. While this means that air masses affecting the study sites in the Philippines mainly pass over the Philippine Sea, some of the backward trajectories suggest that southern Japan could also be a source of atmospheric pollution (e.g. Fig. 1c). As November-April is a period with relatively low precipitation in the Philippines, the chances for rain-out of atmospheric particles are lower, and airborne particles can potentially be transported further. In contrast, during June-September air masses over the Philippines arrive from the west, bringing relatively high amounts of precipitation. The modelling results suggest that there is only limited scope for airborne particle sources from outside of the Philippines to arrive at the study sites on the island of Luzon. Seasonal variability is slightly higher for the sites in Peninsular Malaysia and Singapore. Winds from the northeast dominate from October-January, southwestern winds from January-April, and southeasterly winds from May-September (Supplementary Table 2). Highest amounts of precipitation are commonly observed during the northeast monsoon (November-March) for eastern Peninsular Malaysia, suggesting that although the three-day trajectories cover large distances for these months, reaching as far as the South China Sea and the Indian Ocean (Fig 1c), airborne particles have a higher chance of raining out during this part of the year. The different directions of the air mass trajectories, in addition to the length of the three-day pathways, suggest that the sediment records of our sites represent a regionally integrated signal of air pollution, and that SCPs transported to our site could be partly derived from long-range transport (with travel distances potentially exceeding 10^3 km). However, the modelling results also suggest that for large parts of the year air masses mainly pass over open water, and combined with information on seasonality of precipitation, indicate that most of the airborne particles are probably derived from local sources.

Discussion

Spatio-temporal trends of SCP fluxes

Burning of fossil fuels in SEA started toward the end of the 19th century albeit on a small scale. The first coal-fired power plant in the Philippines was built in Manila, also on the island of Luzon, in 1892 (Ongsotto and Ongsotto, 2002), and this and other power plants constructed in the vicinity of Manila could account for the early detection of SCPs in the record from Sampaloc (Fig. 4), located around 100 km to the south. Extensive and region-wide fossil fuel consumption did not begin until c. 1950-1960, when all four ^{210}Pb-dated records show an increase in SCP flux. The use of fossil fuels was locally stimulated by legislation such as the Oil Exploration and Development Act (1972) of the

Philippines, which offered tax exemptions for oil exploration and exploitation. The increase in coal and oil consumption after 1980 in SEA (Fig. 4b) is mirrored in the increase in SCP flux in the records of Yambo, Sampaloc and Tasik Chini, which all show a phase of SCP flux during the 1980s. A further increase in coal and oil consumption after 2000 (IEA, 2013; Kurokawa et al., 2013) is not reflected in the SCP records, which all show decreasing flux from that time. This divergence in trends might be the result of the implementation of air pollution control measures (Wang et al., 2014; Mohktar et al., 2014). For instance, an expansion of air pollution control measures in the Philippines followed implementation of the Philippines Clean Air Act of 1999 (Republic Act No. 8749), which set pollution emission limitations for the fossil fuel industry (as well as for motor vehicles). Implementation of air pollution control policies commenced in China from 1980 onward, but only became effective from c. 2005 onward (Yin et al., 2016). In Malaysia, the Malaysia Environmental Quality (Clean Air) of 1978 provided the first regulations relating to atmospheric pollution control, only recently being replaced by the New Environmental Quality (Clean Air) Regulation 2014. Despite these intra- and inter-regional differences in the timing of the introduction of air pollution control measures in Southeast and East Asia, their implementation was more strenuously enforced only from c. 2000 onward, and this is in line with our observed decrease in SCP fluxes in SEA.

Historical records of monthly precipitation amounts show a slight increase in rainfall in Malaysia from the 1990s onward (Climate Change Knowledge Portal, http://sdwebx.worldbank.org/climateportal), with the strongest increases in rainfall amounts seen during the northeast monsoon season (November-March). This increase in precipitation amounts could have resulted in more effective rain-out of particulates, and shortened transport distances for airborne particulates such as SCPs (e.g. Ruppel et al., 2013; Supplementary Figure 1). This would have decreased the amount of regionally-derived SCPs for some of our sites from c. 1990. It is however difficult to disentangle the potential effects of an increase in precipitation amounts from the effects of increasingly more effective air pollution control measures, as both would result in decreased SCP fluxes to our sites. More research is needed to differentiate between the effects of these two drivers of changes in SCP deposition at our sites.

Individual SCP flux records were standardised and combined in a regional summary record for SEA (Fig. 4c). The curve that is shown in Fig. 4c is dominated by the results from the Philippines, and is currently based on a relatively low number of records that are available for comparison. Future results from SEA might alter the general trend of the record shown in Fig. 4c. However, the current summary diagram resembles trends observed in extra-tropical parts of Asia, such as China and Japan. For instance, the record for Akani-konuma, a remote high-altitude lake in Japan, shows first occurrences of SCPs around the early 1950s, before reaching peak flux around the late-1980s

(Nagafuchi et al., 2009). SCP concentration data from the middle Yangtze in China show an abrupt increase in the early 1950s, before declining from around 2000, while similar data from Beijing show a much more recent (late 1980s) increase, with the predominant morphology of SCPs indicating the combustion of coal as the main source (Wu et al., 2005; Hirakawa et al., 2011). By comparison, sediment cores from lakes Taihu and Donghu in eastern China both exhibit first occurrences of SCPs in the 1930s before showing rapid increases in SCP deposition around 1950 and peak flux at around 1990 (Rose, 2015). A similar pattern of accumulation is also shown in coastal sediments from Japan (Murakami-Kitase et al., 2010; Hirakawa et al., 2011). Sediment samples from the sub-aqueous part of the Yangtze Delta and dating to before the 1930s contain SCPs, with concentrations rising steeply in the early 1950s (Wang et al., 2014). The similar trends observed in our records and in the published records from Japan and China reflect the simultaneous expansion of fossil fuel combustion around this time. Rose (2015) provides a global synthesis of SCP records, illustrating that while certain parts of the world are well-studied (e.g. Europe), tropical regions are not, hampering our understanding of past atmospheric pollution patterns. Rose (2015) shows a normalised summary curve for Asia that includes 10 sites, but these sites cover a geographical range spanning from the northern Urals in Arctic Russia in the northwest (Solovieva et al., 2005) to Japan in the southeast (Yoshikawa et al., 2000; Nagafuchi et al., 2009), and all are located outside of tropical Asia. The summary curve for Asia (Rose, 2015) shows relatively low abundances or absence of SCPs pre-1950, followed by a trend of increasing flux from the mid-1950s to a peak around 1990. Inferred variations in atmospheric pollution levels for SEA are thus generally in line with information on fossil fuel usage in East and Southeast Asia (Ohara et al., 2007; Wang et al., 2014). While not outside of the range of dating uncertainties there are, however, slight differences in the SCP flux records from the two regions, with peak values being reached in East Asia at c. 1990 (Rose, 2015) but around 2000 in SEA (this study). In addition, the individual records from East Asia show decadal-scale differences when compared with each other as well. On a global scale, most SCP records show a more abrupt increase immediately after c. 1950, reaching peak flux values one or two decades earlier than the peak values as seen in our records. This likely reflects regional differences in development and pollution mitigation.

While future projections of black carbon emissions suggest globally decreasing concentrations, regional estimates differ between a slight increase (Streets et al., 2004) and a decrease (Wang et al., 2014) for SEA. The more recent estimates of a decrease in future emissions take into account substantial measures taken by local governments to reduce air pollution with the objectives of climate change mitigation as well as air quality improvement, such as the Environmental Quality (Clean Air) Regulation of 2014 in Malaysia (Mohktar et al., 2014; Wang et al.,

2014). Our results suggest that strict implementation of these regulations would lead to continued declines in SCP deposition. In contrast, the Philippine Energy Plan (PEP) 2012-2030 seeks to achieve energy independence through the use of indigenous fuel resources, including but not limited to indigenous coal and oil fields. This suggests that the Philippines will remain dependent on conventional fuels for the foreseeable future, thus affecting future SCP emissions in the region.

Potential sources of SCPs

While the patterns of variations in SCP loads are similar between the study sites, the absolute fluxes vary substantially. For instance, our records show that maximum flux at Tasik Chini only reaches 40 cm^{-2} yr^{-1}, whereas maximum flux in the Philippines reaches c. 2000 cm^{-2} yr^{-1}. SCP fluxes can vary over short distances (Rose and Appleby, 2005; Rose, 2015) and catchment- and site-specific processes like wind fetch, exposure, catchment slope, vegetation coverage and sediment transport all influence the extent to which SCPs accumulate in lake sediments, explaining some of the high spatial variability noted in other studies. However, proximity to pollution sources is the most likely explanation for the 2-order magnitude difference observed between our sites. Metropolitan Manila, the capital and by far the largest urban conurbation in the Philippines with an estimated population of 13 million, is located about 100 km to the north of the Seven Crater Lakes. San Pablo (population 266,000), which extends to the shoreline of Sampaloc, is also a relatively large, densely populated urban area. There are several power plants in the air-shed for the cluster of lakes forming the Seven Crater Lakes (Fig. 1b). While smaller-sized power generation facilities have been in operation from 1963 onward, large coal and oil plants came into operation in the 1980s and 1990s. These power plants can serve as local sources of SCPs accumulating in sediments at Mohicap, Sampaloc and Yambo. In contrast, all power plants on Peninsular Malaysia (Fig. 1a) are located on the western side of the peninsula. Tasik Chini therefore receives relatively more long-range emissions than the Philippine sites which receive more short-range transported SCPs.

Mercury fluxes

Global Hg emission rates have tripled since c. 1850, mainly due to increased coal burning (Engstrom et al., 2014; Horowitz et al., 2014). There are however many additional sources of anthropogenic Hg emission, including waste incineration and sulphide ore processing (Hylander and Meil, 2003). An important potential source of atmospheric Hg is artisanal and small-scale gold mining (Mason and Pirrone 2009, Cordy et al., 2010) and an estimated 300,000 people are employed in the small-scale mining sector of the Philippines (Lu, 2012). Artisanal mines have spread throughout the country since the mid-1980s gold-rush, with high numbers on the island of Mindanao to the south of Luzon

(Appleton et al., 1999).The expanding practice of artisanal gold mining in SEA is responsible for much of the region's environmental mercury emissions (Pacyna et al., 2010).

The first significant increases in Hg in lake sediment cores are typically observed from the mid-19th century, even in remote areas (Muir et al., 2009). While our records do not have age-depth models that reach back to the 19th century, our record from Sampaloc shows an increase in Hg concentrations at c. 65 cm depth. We interpret this increase in concentration as a clear pollution signal, which occurred prior to c. 1925 (37 cm depth), the start of our chronology. The declining trend in Hg concentrations at Sampaloc is related to dilution as a result of increased sedimentation rates, as Hg flux increases from c. 1925 (Fig. 5). Similarly, Hg concentrations at Yambo increase from 85 cm onward, which is sometime before the c. 1950 (47 cm depth) onset of the sediment chronology for this site. The observed values of c. 40-110 µg m^{-2} yr^{-1} compare well to modern observations of wet deposition fluxes of total Hg in China, which ranges between 24.9 and 39.6 µg m^{-2} yr^{-1} for five study sites in the Wujiang River basin, but are much higher than observations of wet deposition fluxes for Europe and North America (Guo et al., 2008; Yang et al., 2009). However, comparison of fluxes derived from different types of observations as well as from different areas will be hampered by the difference in sources of input, as well as differences in the human impact on the landscape (e.g. deforestation). While the SCPs encountered in our records might reflect a local or regional source of pollution, the early increases in Hg concentrations most likely indicate a larger regional or even global impact, in line with observations elsewhere (Fitzgerald et al., 2005; Muir et al., 2009; Yang et al., 2010). The presence of artisanal gold mining as well as other small-scale mining activities will likely have provided additional local inputs of Hg.

Impact of atmospheric pollution on Southeast Asian wetlands

Lakes and wetland ecosystems are not equally vulnerable to pollution because of their differing ability to buffer the effects of pollutants, but little is known of the buffering capacity of aquatic ecosystems in SEA. Alkalinity of waters from Tasik Chini is rather low (0.05-0.20 meq L^{-1}; unpubl. data), and thus poorly buffered and susceptible to acidification. The results of a region-wide precipitation monitoring project show that precipitation has an annual average pH of <5.0 for large parts of SEA, with sulphuric acid the main cause of acidification (EANET, 2011). Lake monitoring data for sites in Malaysia and Indonesia provide evidence for declining lake-water pH and increasing sulphate (SO_4^{2-}) concentration, although the cause of apparent acidification remains unknown (EANET, 2011; Sase et al., 2017). Combined with other pressures on water quality (e.g. sewerage inputs from urban areas, fish farming, catchment disturbance, climate change), acidification poses a

severe risk to aquatic ecosystem functioning and service provision in SEA, and indeed tropical Asia more widely.

SCP fluxes in SEA have declined over the last two decades (Fig. 4), likely as a result of the introduction of particle-arrestor technologies and improved pollution mitigation policies for industrial fuel combustion. In contrast, Hg fluxes at these lakes (Fig. 5) have remained relatively constant across the second half of the 20th century to the present. Hg concentrations show a decreasing trend in Sampaloc, potentially related to dilution through increased sedimentation rates, and have remained stable at Yambo, despite the observed increase in sedimentation rates. While several pollution controls have constrained emissions of atmospheric Hg from e.g. power generation and cement production (Zhao et al., 2015), the more diverse sources of Hg, including artisanal mining, might explain the absence of a decrease in sedimentary Hg concentrations in the Yambo record.

The increased sedimentation rates at Sampaloc and Yambo could partially reflect elevated levels of catchment soil erosion. This soil material includes Hg from atmospheric deposition over time, and is thus a source of delayed input of Hg (Yang et al., 2016). Hg flux to these lakes can therefore be expected to remain high for decades to come, even following the implementation of mitigation measures such as those associated with the Minamata Convention (Ha et al., 2017). Transfer of Hg may therefore have potentially long-lasting impacts on aquatic and human health.

Conclusions

We used lake sediment archives to reconstruct trends in atmospheric pollution levels across SEA, covering the period from the start of industrial fuel consumption to the present. First occurrences of SCPs, reflecting early developments in the industrial combustion of coal and oil, are dated to c. 1950 at Tasik Chini (Malaysia) and are shown to predate c. 1925 at Sampaloc (Philippines). All SCP records show increasing fluxes from 1960 onward, indicating the onset of extensive and region-wide fossil fuel consumption. Increases in SCP fluxes between 1960 and 2000 reflect the increases in fossil fuel consumption in SEA, whereas the decreasing SCPs fluxes between 2000 and the present might be the result of the implementation of air pollution control measures. Atmospheric modelling suggests that most of the airborne particles are derived from local or regional sources. The trends observed in our SCP flux data compare well to independent records from extra-tropical parts of Asia, although peak flux is reached slightly later in SEA (around 2000) when compared to records from China and Japan (c. 1990).

The Sampaloc record shows an increase in Hg concentrations prior to c. 1925, the start of our chronology, which is interpreted as a clear pollution signal. Both the Sampaloc and the Yambo

record show relatively high Hg fluxes with maximum fluxes reaching 90-110 µg m^{-2} yr^{-1}. The reconstructed fluxes compare well to observations from China, but are higher than recent Hg deposition rates observed in Europe and North America. Whereas the SCPs encountered in our records might reflect a regional source of pollution, the early increases in Hg concentrations most likely indicate a larger regional or even global impact. The extensive presence of artisanal mining activities in the Philippines will likely have provided additional local inputs of Hg.

Acknowledgements

Thanks are due to staff and students in the Research Center for the Natural and Applied Sciences, University of Santo Tomas, Manila, Philippines, for assistance in the field, and to the Public Utilities Board (PUB), Singapore, for permission to carry out fieldwork at UPR and also for assistance with fieldwork. Particular thanks are due to Rey Donna Papa and to Loh Sze Sian. We would also like to thank Virginia Panizzo and Wayne Bannister for logistic support, Keely Mills for advice during the design of the Tasik Chini research project, and Sarah Metcalfe for helpful comments on an earlier draft of the manuscript. Finally, we are grateful for the very constructive comments on an earlier version of this manuscript from three anonymous reviewers.

Supporting Information. Table S1 presents site information for the five study sites presented in this manuscript. Table S2 provides information on monthly wind (Table S2a) and precipitation (Table S2b) amounts for Singapore, Malaysia and the Philippines. Table S3 provides the ^{210}Pb measurement data for the four radiometrically dated profiles. Figure S1 shows altitudes of air masses during the 72 hours prior to arriving at our sites for five selected dates (cf the data shown in Fig. 1c-11g)

References

Akimoto H (2003) Global air quality and pollution. Science 302, 1716-1719.

Amann M, Klimont Z, Wagner F (2013) Regional and Global Emissions of Air Pollutants: Recent Trends and Future Scenarios. Annu. Rev. Environ. Resour. 38, 31−55.

Appleby PG, Nolan PJ, Gifford DW, Godfrey MJ, Oldfield F, Anderson NJ, Battarbee RW (1986) ^{210}Pb dating by low background gamma counting. Hydrobiologia 141, 21-27.

Appleby PG (2001) Chronostratigraphic techniques in recent sediments. In Tracking Environmental Change Using Lake Sediments. Vol. 1: Basin Analysis, Coring and Chronological Techniques; Last, W. M., Smol, J. P., Eds.; Kluwer: Dordrecht; pp 171−203.

522 Appleton JD, Williams TM, Breward N, Apostol A, Miguel J, Miranda C (1999) Mercury contamination
523 associated with artisanal gold mining on the island of Mindanao, the Philippines. Sci. Total
524 Environ. 228, 95-105.
525 Aquino LV (1983) Using Spheroidal Carbonaceous Particles in lake sediments as a stratigraphic
526 marker for the Anthropocene, Philippines. M.Sc. Dissertation, University of the Philippines,
527 Iloilo City, Philippines.
528 Azimi S, Moghaddam MS (2013) Effect of mercury pollution on the urban environment and human
529 health. Environ. Ecol. Res. 1, 12-20.
530 Barst BD, Ahad JME, Rose NL, Jautzy JJ, Drevnick PE, Gammon PR, Sanei H, Savard MM (2017) Lake-
531 sediment record of PAH, mercury, and fly-ash particle deposition near coal-fired power
532 plants in Central Alberta. Environ. Pollut. 231, 644-653.
533 Bindler R, Renberg I, Appleby PG, Anderson NJ, Rose NL (2001) Mercury accumulation rates and
534 spatial patterns in lake sediments from west Greenland: a coast to ice margin transect.
535 Environ. Sci. Technol. 35, 1736-1741.
536 Brillo BBC (2016) Developing Mohicap Lake, San Pablo City, Philippines. Soc. Sci. 11, 283-290.
537 Chirinos L, Rose NL, Urrutia R, Muñoz P, Torrejón PF, Torres L, Cruces F, Araneda A, Zaror C (2006)
538 Environmental evidence of fossil fuel pollution in Laguna Chica de San Pedro lake sediments
539 (Central Chile). Environ. Pollut. 141, 247-256.
540 Cordy P, Veiga MM, Salih I, Al-Saadi S, Console S, Garcia O, Mesa LA, Velásquez-López PC, Roeser M
541 (2011) Mercury contamination from artisanal gold mining in Antioquia, Colombia: The
542 world's highest per capita mercury pollution. Sci. Total Environ. 410-411, 154-160.
543 EANET (2011) *The second periodic report on the state of acid deposition in East Asia*; Acid Deposition
544 Monitoring Network in East Asia. Acid Deposition Monitoring Network in East Asia (EANET)
545 EANET (2015) *Review on the State of Air Pollution in East Asia*. Acid Deposition Monitoring Network
546 in East Asia (EANET)
547 Engstrom DR, Fitzgerald WF, Cooke CA, Lamborg CH, Drevnick PE, Swain EB, Balogh SJ, Balcom PH
548 (2014) Atmospheric Hg emissions from preindustrial gold and silver extraction in the
549 Americas: A reevaluation from lake-sediment archives. Environ. Sci. Technol. 48, 6533-6543.
550 Fitzgerald WF, Engstrom DR, Lamborg CH, Tseng CM, Balcom PH, Hammerschmidt CR (2005) Modern
551 and historic atmospheric mercury fluxes in northern Alaska: global sources and Arctic
552 depletion. Environ. Sci. Technol. 39, 557-568.
553 Fu C, Ding A, Wu J (2017) Review on Studies of Air Pollution and Climate Change Interactions in
554 Monsoon Asia. In: Chang C-P, Kuo H-C, Lau N-C, Johnson RH, Wheeler MC (Eds) *The Global*
555 *Monsoon System: Research and Forecast 9*. pp 315-327.

556 Guo Y, Feng X, Li Z, He T, Yan H, Meng B, Zhang J, Qiu G (2008) Distribution and wet deposition fluxes
557 of total and methyl mercury in Wujiang River Basin, Guizhou, China. Atmosph. Environ. 42,
558 7096-7103.
559 Ha E, Basu N, Bose-O'Reilly S, Dorea JG, McSorley E, Sakamoto M, Chan HM (2017) Current progress
560 on understanding the impact of mercury on human health. Environ. Res. 152, 419-433.
561 Hirakawa H, Muralami-Kitase A, Okudaira T, Inoue J, Yamazak H, Yoshikawa S (2011) The spatial and
562 temporal distributions of spheroidal carbonaceous particles from sediment core samples
563 from industrial cities in Japan and China. Environ. Earth Sci. 64, 833-840
564 Horowitz HM, Jacob DJ, Amos HM, Streets DG, Sunderland EM (2014) Historical Mercury Releases
565 from Commercial Products: Global Environmental Implications. Environ. Sci. Technol. 48,
566 10242-10250.
567 Hylander LD, Meil IM (2003) 500 years of mercury production: global annual inventory by region
568 until 2000 and associated emissions. Sci. Total Environ. 304, 13-27.
569 Inoue J, Momose A, Okudaira T, Murakami-Kitase A, Yamazaki H, Yoshikawa S (2014) Chemical
570 compositions of Northeast Asian fly ash particles: Implications for their long-range
571 transportation. Atmos. Environ. 95, 375-382.
572 Intergovernmental Panel on Climate Change (2014) *Climate Change 2014: Synthesis Report*.
573 Contribution of Working Groups I, II and III to the Fifth Assessment Report of the
574 Intergovernmental Panel on Climate. Geneva, Switzerland.
575 International Energy Agency (2013) *Southeast Asia Energy Outlook. World Energy Outlook Special*
576 *Report*. Paris, France.
577 International Energy Agency (2016) *Energy and air pollution. World Energy Outlook – Special report*.
578 Paris, France.
579 Jacobson MZ (2001) Strong radiative heating due to the mixing state of black carbon in atmospheric
580 aerosols. Nature 409, 695– 697.
581 Kato N, Akimoto H (1992) Anthropogenic emissions of SO_2 and NO_x in Asia: emissions inventories,
582 Atmos. Environ. 26, 2997–3017.
583 Klimont Z, Smith SJ, Cofala J (2013) The last decade of global anthropogenic sulfur dioxide:
584 2000–2011 emissions. Environ. Res. Lett. 8, 014003.
585 Kopf RK, Finlayson CM, Humphries P, Sims NC, Hladyz S (2015) Anthropocene baselines: assessing
586 change and managing biodiversity in human-dominated aquatic ecosystem. Biosci 65, 798-
587 811.
588 Koplitz SN, Mickley LJ, Marlier ME, Buonocore JJ, Kim PS, Liu T, Sulprizio MP, DeFries R, Jacob DJ,
589 Schwartz J, Pongsiri M, Myers S (2016) Public health impacts of the severe haze in Equatorial

590 Asia in September–October 2015: demonstration of a new framework for informing fire
591 management strategies to reduce downwind smoke exposure. Environ. Res. Lett. 11,
592 094023.
593 Koplitz SN, Jacobs DJ, Sulprizio MP, Myllyvirta L, Reid C (2017) Burden of Disease from Rising Coal-
594 Fired Power Plant Emissions in Southeast Asia. Environ. Sci. Technol. 51, 1467-1476.
595 Kubota H, Chan JCL (2009) Interdecadal variability of tropical cyclone landfall in the Philippines from
596 1902 to 2005. Geophys. Res Lett. 36, L12802.
597 Kurokawa J, Ohara T, Morikawa T, Hanayama S, Janssens-Maenhout G, Fukui T, Kawashima K,
598 Akimoto H (2013) Emissions of air pollutants and greenhouse gases over Asian regions
599 during 2000-2008: Regional Emission inventory in Asia (REAS) version 2. Atmos. Chem. Phys.
600 13, 11019-11058.
601 Laguna Lake Development Authority-Environmental Quality Management Division (2008) *Water*
602 *Quality Report of the Seven Crater Lakes 2006-2008.* Rizal, Philippines.
603 Lai I-C, Lee C-L, Huang H-C (2016) A new conceptual model for quantifying transboundary
604 contribution of atmospheric pollutants in the East Asia Pacific rim region. Environ. Internat.
605 88, 160-168.
606 Lau KM, Kim MK, Kim KM (2006) Asian summer monsoon anomalies induced by aerosol direct
607 forcing: The role of the Tibetan Plateau. Clim. Dynam. 26, 855–864.
608 Lu JL (2012) Occupational health and safety in small scale mining: focus on women workers in the
609 Philippines. J Internat. Women's Studies 13, 103-113.
610 Mason R, Pironne N (2009) *Mercury Fate and Transport in the Global Atmosphere Emissions,*
611 *Measurements and Models.* Springer US, New York
612 Mohktar MM, Taib RM, Hassim MH (2014) Understanding selected trace elements behavior in a
613 coal-fired power plant in Malaysia for assessment of abatement technologies. J Air & Waste
614 Manag. Assoc. 64, 867–878.
615 Mott R, Herrod A, Clarke RH (2017) Post-breeding dispersal of frigatebirds increases their exposure
616 to mercury. Mar. Pollut. Bull. 119, 204-210.
617 Muir DCG, Wang X, Yang F, Nguyen N, Jackson TA, Evans MS, Douglas M, Kock G, Lamoureux S,
618 Pienitz R, Smol JP, Vincent WF, Dastoor A (2009) Spatial trends and historical deposition of
619 mercury in eastern and northern Canada inferred from lake sediment cores. Environ. Sci.
620 Technol. 43, 4802-4809.
621 Murakami-Kitase A, Okudaira T, Inoue J, (2010) Relationship between surface morphology and
622 chemical composition of spheroidal carbonaceous particles within sediment core samples
623 recovered from Osaka Bay Japan. Environ. Earth Sci. 59, 1723–1729

624 Nagafuchi O, Rose NL, Hoshika A, Satake K (2009) The temporal record and sources of
625 atmospherically deposited fly-ash particles in Lake Akagi-konuma, a Japanese mountain lake.
626 J. Paleolimnol. 42, 359-371.
627 Ohara T, Akimoto H, Kurokawa J, Horii N, Yamaji K, Yan X, Hayasaka T (2007) An Asian emission
628 inventory of anthropogenic emission sources for the period 1980-2020. Atmosph. Chem.
629 Phys. 7, 4419-4444.
630 Okelsrud A, Lydersen E, Fjeld E (2016) Biomagnification of mercury and selenium in two lakes in
631 southern Norway. Sci. Total Environ. 566, 596-607.
632 Ongsotto RR, Ongsotto RR (2002) Philippine history module-based learning, 1st ed; Rex Book Store:
633 Manilla.
634 Pacyna EG, Pacyna JM, Sundseth K, Munthe J, Kindbom K, Wilson S, Steenhuisen F, Maxson P (2010)
635 Global emission of mercury to the atmosphere from anthropogenic sources in 2005 and
636 projections to 2020. Atmosph. Environ. 44, 2487-2499.
637 Pittauerová D, Hettwig B, Fischer HW (2011) Pb-210 sediment chronology: Focused on supported
638 lead. Radioprotection 46, S277-S282.
639 Ramanathan V, Chung C, Kim D, Bettge T, Buja L, Kiehl JT, Washington WM, Fu Q, Sikka DR, Wild M
640 (2005) Atmospheric brown clouds: impact on South Asian climate and hydrologic cycle. P.
641 Natl. Acad. Sci. 102, 5326–5333.
642 Rice KM, Walker EM Jr, Wu M, Gillette C, Blough ER (2014) Environmental mercury and its toxic
643 effects. J. Prev. Med. Public Health 47, 74-83.
644 Richter A, Burrows P, Nues H, Granier C, Niemeijer U (2005) Increase in tropospheric nitrogen
645 dioxide over China observed from space. Nature 437, 129–130.
646 Robbins JA (1978) Geochemical and geophysical applications of radioactive lead. Biogeochem. Lead
647 Environ. 1, 285-337.
648 Rose NL (1994) A note on further refinements to a procedure for the extraction of carbonaceous fly
649 ash particles from sediments. J. Paleolimnol. 11, 201–204.
650 Rose NL (2001) Fly ash particles. In: Tracking Environmental Change Using Lake Sediments, Vol. 2.
651 Physical and Chemical Techniques; Last, W. M., Smol, J. P., Eds.; Kluwer Academic Publishers:
652 Dordrecht, pp. 319–349.
653 Rose NL (2008) Quality control in the analysis of lake sediments for spheroidal carbonaceous
654 particles. Limnol. Oceanogr. Methods 6, 172-179.
655 Rose NL (2015) Spheroidal Carbonaceous Fly Ash Particles Provide a Globally Synchronous
656 Stratigraphic Marker for the Anthropocene. Environ. Sci. Technol. 49, 4155-4162.

Rose NL, Appleby PG (2005) Regional applications of lake sediment dating by spheroidal carbonaceous particle analysis I. United Kingdom. J. Paleolimnol. 34, 349-361.

Rose NL, Juggins S (1994) A spatial relationship between carbonaceous particles in lake sediments and sulphur deposition. Atmosph. Environ. 28, 177-183.

Rose NL, Juggins S, Watt J, Battarbee R (1994) Fuel-type characterisation of spheroidal carbonaceous particles using surface chemistry. Ambio. 23, 296-299.

Rose NL, Appleby PG, Boyle JF, Mackay AW, Flower RJ (1998) The spatial and temporal distribution of fossil-fuel derived pollutants in the sediment record of Lake Baikal, eastern Siberia. J. Paleolimnol. 20, 151-162.

Rose NL, Flower RJ, Appleby PG (2003) Spheroidal carbonaceous particles (SCPs) as indicators of atmospherically deposited pollutants in North African wetlands of conservation importance. Atmosph. Environ. 37, 1655–1663.

Rose NL, Jones VJ, Noon PE, Hodgson DA, Flower RJ, Appleby PG (2012) Long-range transport of pollutants to the Falkland Islands and Antarctica: Evidence from lake sediment fly-ash particle records. Environ. Sci. Technol. 46**,** 9881-9889.

Ruppel M, Lund MT, Grythe H, Rose NL, Weckström J, Korhola A (2013) Comparison of Spheroidal Carbonaceous Particle Data with Modelled Atmospheric Black Carbon Concentration and Deposition and Air Mass Sources in Northern Europe, 1850–2010. Adv. Meteorol. 2013, Article ID 393926, http://dx.doi.org/10.1155/2013/393926.

Sase H, Yamashita N, Luangjame J, Garivait H, Kietvuttinon B, Visaratana T, Kamisako M, Kobayashi R, Ohta S, Shindo J, Hayashi K, Toda H, Matsuda K (2017) Alkalinization and acidification of stream water with changes in atmospheric deposition in a tropical dry evergreen forest of northeastern Thailand. Hydrol. Proc. 31, 836–846.

Schroeder WH, Munthe J (1998) Atmospheric mercury – an overview. Atmosph. Environ. 32, 809-822.

Sharip Z, Jusoh J (2010) Integrated lake basin management and its importance for Lake Chini and other lakes in Malaysia. Lakes Reservoirs: Res. Manag. 15, 41–51.

Sharip Z, Zaki ATA, Shapai MAHM, Suratman S, Shaaban AJ (2014) Lakes of Malaysia: Water quality, eutrophication and management. Lakes Reservoirs: Res. Manag. 19, 130–141.

Shotyk W, Appleby PG, Bicalho B, Davies LJ, Froese D, Grant-Weaver I, Magnan G, Mullan-Boudreau G, Noemberg T, Pelletier R, Shannon B, van Bellen S, Zaccone C (2017) Peat bogs document decades of declining atmospheric contamination by trace metals in the Athabasca Bituminous Sands Region. Environ. Sci. Technol. 51, 6237-6249.

690 Shuhaimi-Othman M, Eng CL, Idris M (2007) Water Quality Changes in Chini Lake, Pahang, West
691 Malaysia. Environ. Monit. Assess. 131, 279–292.
692 Solovieva N, Jones VJ, Nazarova L, Brooks SJ, Birks HJB, Grytnes J-A, Appleby PG, Kauppila T,
693 Kondratenok BM, Renberg I, Ponomarev V (2005) Palaeolimnological evidence for recent
694 climatic change in lakes from the northern Urals, arctic Russia. J. Paleolimnol. 33, 463-482.
695 Stein AF, Draxler RR, Rolph GD, Stunder BJB, Cohen MD, Ngan F (2015) NOAA's HYSPLIT atmospheric
696 transport and dispersion modelling system. Bull. Amer. Meteor. Soc. 96, 2059-2077.
697 Stockholm International Water Institute (2009) *Securing water for ecosystem and human well-being:*
698 *the importance of environmental flows*. Swedish Water House Report 24. Stockholm,
699 Sweden.
700 Streets DG, Bond TC, Carmichael GR, Fernandes SD, Fu Q, He D, Klimont Z, Nelson SM, Tsai NY, Wang
701 MQ, Woo J-H, Yarber KF (2003) An inventory of gaseous and primary aerosol emissions in
702 Asia in the year 2000, J. Geophys. Res., 108, 8809.
703 Streets DG, Bond TC, Lee T, Jang C (2004) On the future of carbonaceous aerosol emissions. J.
704 Geophys. Res. 109, D24212.
705 Wang SX, Zhao B, Cai SY, Klimont Z, Nielsen CP, Morikawa T, Woo JH, Kim Y, Fu X, Xu JY, Hao JM, He
706 KB (2014) Emission trends and mitigation options for air pollutants in East Asia. Atmos.
707 Chem. Phys. 14, 6571–6603.
708 Wang ZH, Dong YH, Chen J, Li XF, Cao J, Deng ZY (2014). Dating recent sediments from the
709 subaqueous Yangtze Delta and adjacent continental shelf, China. J. Palaeogeog. 3, 207-218.
710 World Health Organisation Press (2016) *World health statistics 2016. Monitoring for the Sustainable*
711 *Development Goals*. Geneva, Switzerland.
712 Wu YH, Wang SM, Xia WL, Liu J (2005) Dating recent lake sediments using spheroidal carbonaceous
713 particle (SCP). Chin. Sci. Bull. 50, 1016-1020.
714 Yang H, Rose NL, Battarbee RW (2001) Dating of recent catchment peats using spheroidal
715 carbonaceous particle (SCP) concentration profiles with particular reference to Lochnagar,
716 Scotland. Holocene 11, 593-597.
717 Yang H, Berry A, Rose N, Berg T (2009) Decline in atmospheric mercury deposition in London. J.
718 Environ. Monit. 11, 1518-1522.
719 Yang, H, Battarbee, RW, Turner, SD, Rose, NL, Derwent, RG, Wu, G, Yang R (2010). Historical
720 reconstruction of mercury pollution across the Tibetan Plateau using lake sediments.
721 Environ. Sci. Technol. 44, 2918-2924.
722 Yang H, Turner S, Rose NL (2016) Mercury pollution in the lake sediments and catchment soils of
723 anthropogenically-disturbed sites across England. Environ. Pollut. 219, 1092-1101.

Yin J, Andersson H, Zhang S (2016) Air Pollution Control Policies in China: A Retrospective and Prospects. Intern. J. Environ. Res. Publ. Health 13, 1219

Yoshikawa S, Yamaguchi S, Hata A (2000) Paleolimnological investigation of recent acidity changes in Sawanoike Pond, Kyoto, Japan. J. Paleolimnol. 23, 285-304.

Zhao Y, Zhong H, Zhang J, Nielsen CP (2015) Evaluating the effects of China's pollution controls on inter-annual trends and uncertainties of atmospheric mercury emissions. Atmos. Chem. Phys. 15, 4317–4337.

Figures

Fig. 1: a-b) Map of sites and locations of power plants. SCL = Seven Crater Lakes (Philippines); TC = Tasik Chini (Malaysia); SR = Singapore Reservoir (Singapore). Only power plants that started operations prior to 2000 are shown for the Philippines; c-g) 3-day isobaric backward trajectories ending at our study sites: Blue: air masses reaching the sites in the Philippines; green: air masses reaching Tasik Chini (Malaysia); red: air masses reaching Singapore. Orange arrows summarise seasonal wind directions based on the data shown in Supplementary Table 2, with panels showing characteristic months that exemplify the seasonal (monsoonal) variability in wind directions in SEA. Basemaps for (a) and (b) from www.freevectormaps.com

Fig. 2: Radiometric chronologies for the four dated records: Lake Mohicap, Lake Sampaloc, Lake Yambo (all Philippines) and Tasik Chini (Malaysia) showing the CRS model ^{210}Pb dates and age (solid lines) as well as the sedimentation rates (dashed lines)

Fig. 3: SCP concentrations for Lake Mohicap, Sampaloc and Yambo (Philippines), Lake Tasik Chini (Malaysia) and a reservoir in Singapore (SR). Concentrations as number of particles per gram dry material (n gDM^{-1})

Fig. 4: A. SCP fluxes for Lake Mohicap, Sampaloc and Yambo (Philippines) and Lake Tasik Chini (Malaysia) expressed as numbers of particles per cm^2 per year (n cm^{-2} yr^{-1}). B. Coal (10^3 short tonnes; ST) and oil (10^3 barrels/day; bd^{-1}) usage in selected SEA countries since 1980 (www.eia.gov) C. Summary diagram for SEA with SCP sediment profile data from (a) normalized to the SCP accumulation peak (1.0) for the individual sites. Open circles reflect individual data points; the red line represents a general trend and is calculated by applying a LOESS smoother (span = 0.15) to the data. Horizontal bar indicates 1950 ± 5 years representing the global increase in SCP contamination during the mid-20th century (Rose 2015)

758

759 Fig. 5: SCP and Hg concentrations and fluxes for (a) Lake Sampaloc and (b) Lake Yambo (Philippines).
760 Concentration curves on a depth (cm) scale; fluxes on an age scale with a secondary depth scale
761 plotted for comparison

Figure 1

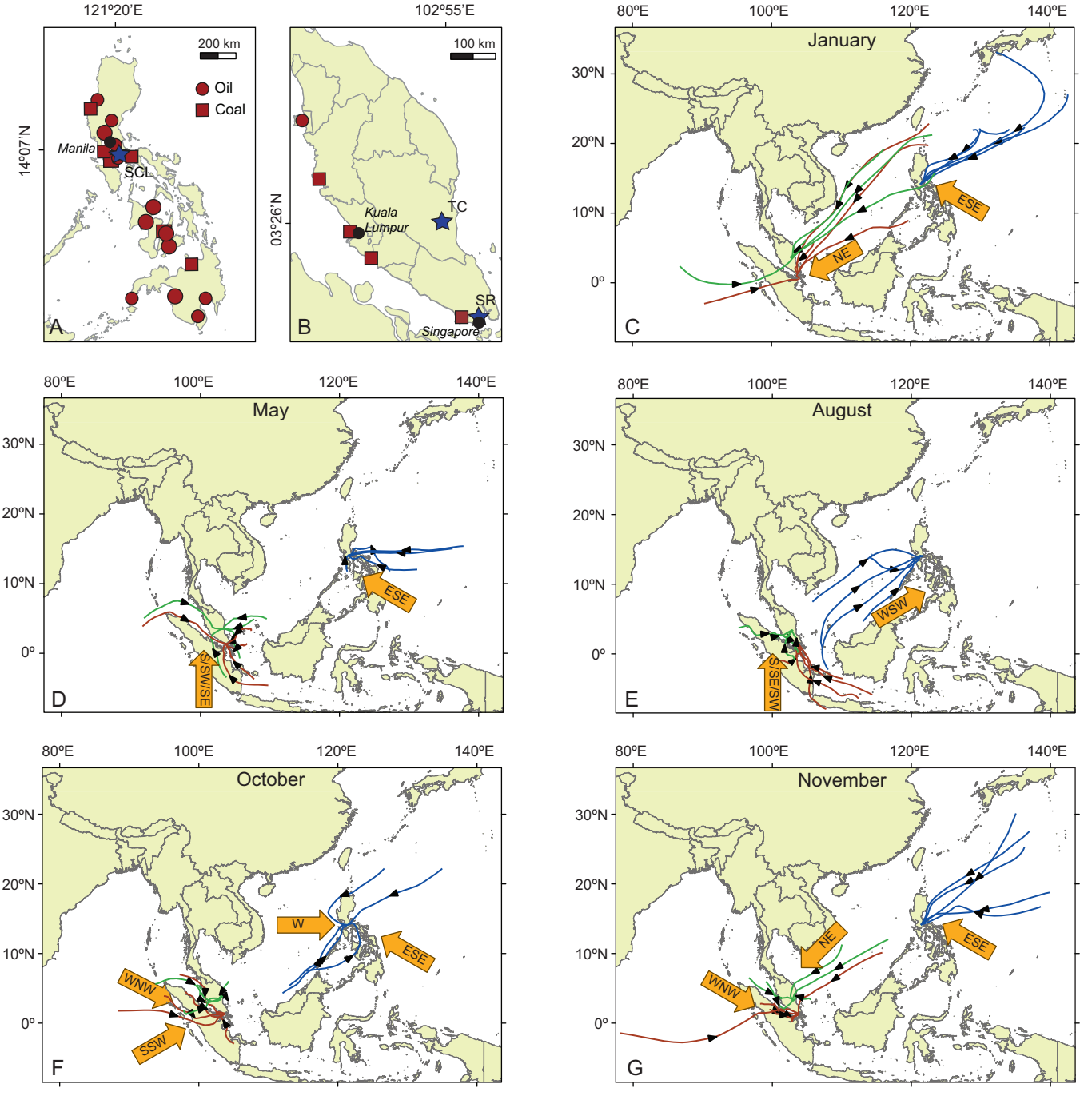

Fig. 1: a-b) Map of sites and locations of power plants. SCL = Seven Crater Lakes (Philippines); TC = Tasik Chini (Malaysia); SR = Singapore Reservoir (Singapore). Only power plants that started operations prior to 2000 are shown for the Philippines; c-g) 3-day isobaric backward trajectories ending at our study sites: Blue: air masses reaching the sites in the Philippines; green: air masses reaching Tasik Chini (Malaysia); red: air masses reaching Singapore. Orange arrows summarise seasonal wind directions based on the data shown in Supplementary Table 2, with panels showing characteristic months that exemplify the seasonal (monsoonal) variability in wind directions in SEA. Basemaps for (a) and (b) from www.freevectormaps.com

Figure 2

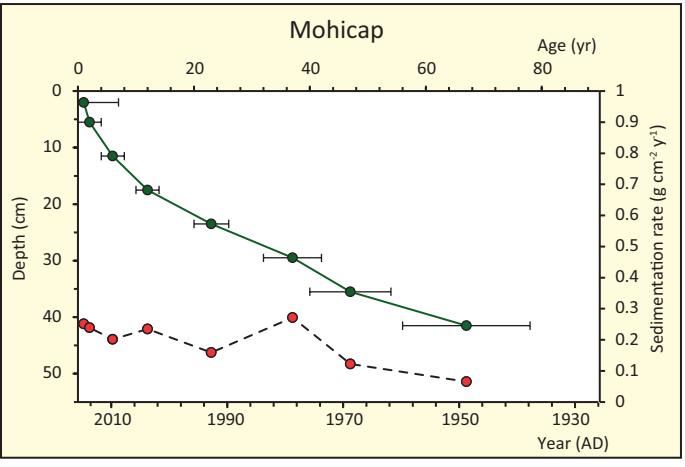

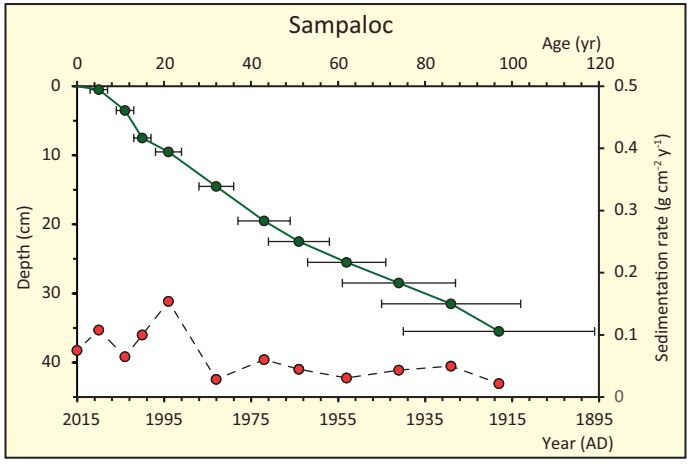

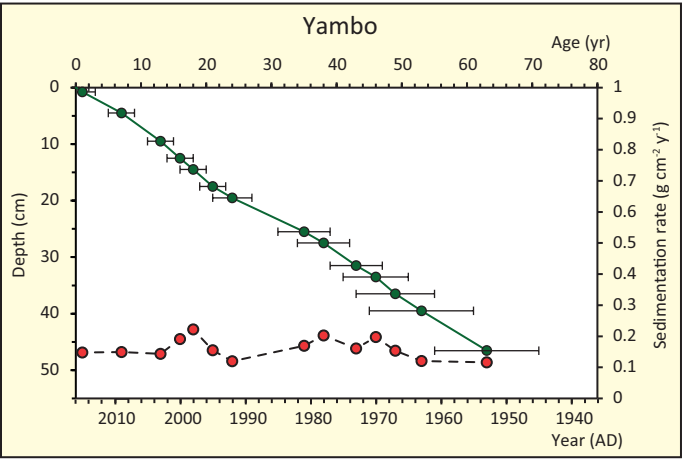

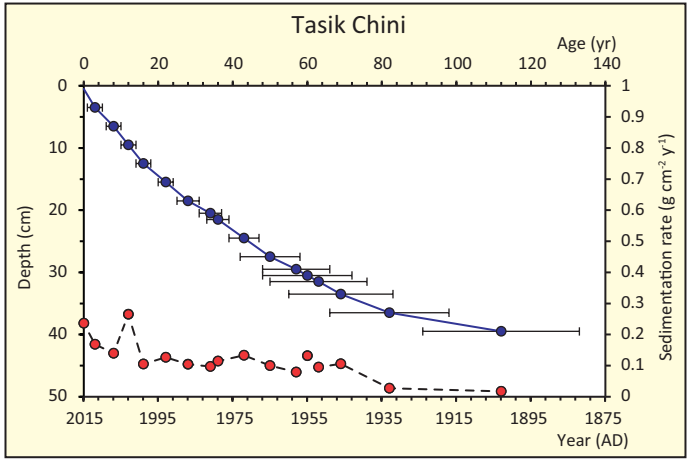

Fig. 2: Radiometric chronologies for the four dated record: Lake Mohicap, Lake Sampaloc, Lake Yambo (all Philippines) and Tasik Chini (Malaysia) showing the CRS model ^{210}Pb dates and age (solid lines) as well as the sedimentation rates (dashed lines)

Figure 3

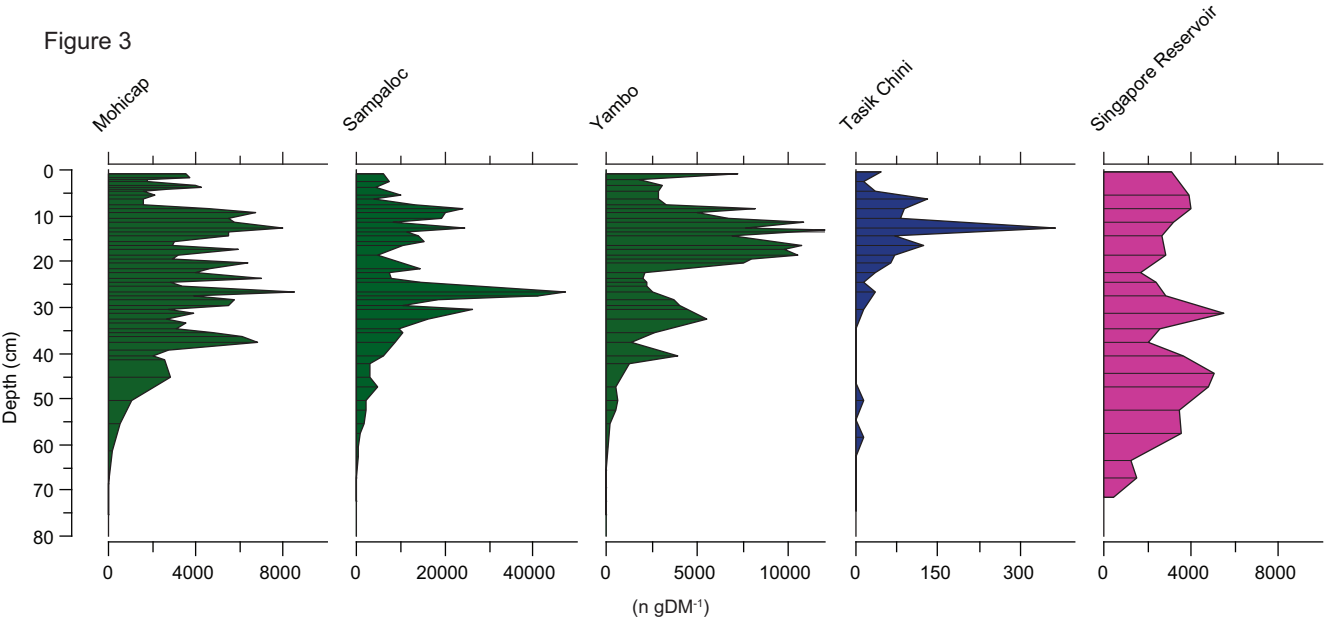

Fig. 3: SCP concentrations for Lake Mohicap, Sampaloc and Yambo (Philippines), Lake Tasik Chini (Malaysia) and a reservoir in Singapore (SR). Concentrations as number of particles per gram dry material (n gDM^{-1})

Figure 4

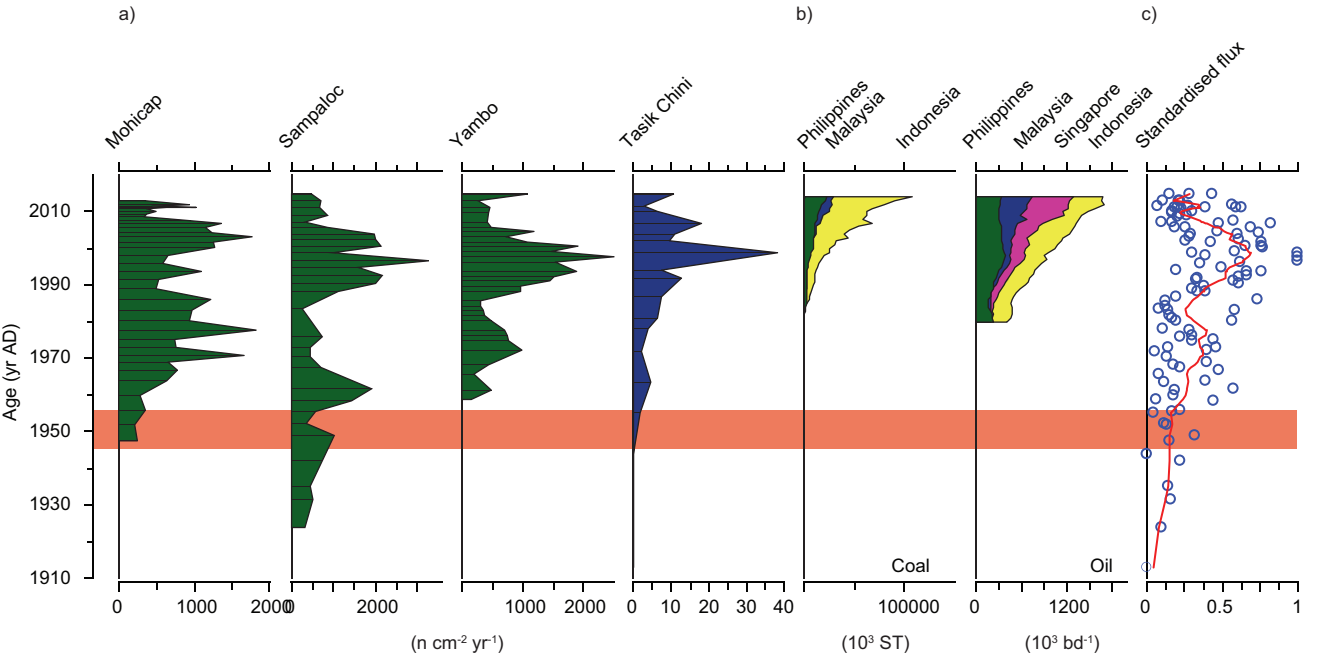

Fig. 4: A. SCP fluxes for Lake Mohicap, Sampaloc and Yambo (Philippines) and Lake Tasik Chini (Malaysia) expressed as numbers of particles per cm^2 per year (n cm^{-2} yr^{-1}). B. Coal (10^3 short tonnes; ST) and oil (10^3 barrels/day; bd^{-1}) usage in selected SEA countries since 1980 (www.eia.gov) C. Summary diagram for SEA with SCP sediment profile data from (a) normalized to the SCP accumulation peak (1.0) for the individual sites. Open circles reflect individual data points; the red line represents a general trend and is calculated by applying a LOESS smoother (span = 0.15) to the data. Horizontal bar indicates 1950 ± 5 years representing the global increase in SCP contamination during the mid-20th century (Rose 2015)

Figure 5

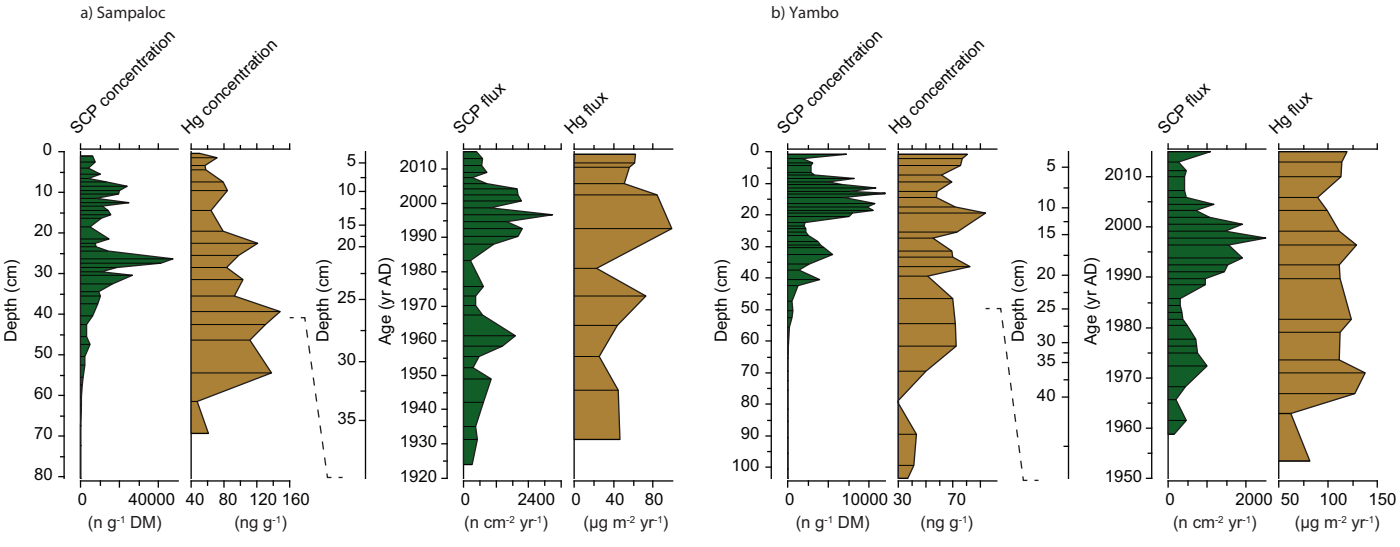

Fig. 5: SCP and Hg concentrations and fluxes for (a) Lake Sampaloc and (b) Lake Yambo (Philippines). Concentration curves on a depth (cm) scale; fluxes on an age scale with a secondary depth-scale plotted for comparison

Supplementary information

Table S1: Site information. Surface area is an approximation as this will seasonally vary for some of the sites. Water depths as recorded at time of coring.

Site	Latitude (N)	Longitude (E)	Altitude (m)	Surface area (km^2)	Water depth (m)	Lake type	Length obtained core (cm)
Philippines							
Mohicap	14°07'19"	121°20'03"	99	0.23[a)]	30.4	Crater lake	87
Sampaloc	14°04'44"	121°19'47"	108	1.04[a)]	27.6	Crater lake	81
Yambo	14°07'09"	121°21'59"	207	0.30[a)]	38.0	Crater lake	104
Malaysia							
Tasik Chini	03°26'01"	102°55'43.1"	12	2.0[b)]	2.5	Floodpulse wetland	75
Singapore							
Reservoir	01°22'13"	103° 48'11"	42	3.2[c)]	7.8	Reservoir	72

a) Brillo BBC (2016) Developing Mohicap Lake, San Pablo City, Philippines. Soc. Sci. 11, 283-290.
b) Shuhaimi-Othman M, Eng CL, Idris M (2007) Water Quality Changes in Chini Lake, Pahang, West Malaysia. Environ. Monit. Assess. 131, 279–292.
c) Public Utilities Board Website; http://www.pub.gov.sg/abcwatersIM/upper-peirce.html

Table S2: Monthly measurements of wind directions and precipitation amounts for each of our study areas. Color codes in table 2a indicate time intervals with similar wind conditions. Black boxes indicate months selected for backward trajectory modelling

Table S2a. Monthly wind patterns

	Jan	Feb	Mar	Apr	May	Jun	Jul	Aug	Sep	Oct	Nov	Dec
Philippines	ESE	ESE	ESE	ESE	WSW-ESE	WSW-ESE	WSW-ESE	WSW	WSW	WSW-ESE	ESE	ESE
Malaysia	SW-NE	SW-NE	SW-NE	SW-NE	SSE	SSE	SSE	SSE	SSE	WNW-SSW	WNW-NNE	NW-NE
Singapore	NE	NE	NE	NE	SSW	SSW	SSW	SSW	SSW	SSW	NE	NE

Wind directions retrieved from the freely available data on:
https://www.windfinder.com/windstatistics/manila_airport
https://www.windfinder.com/windstatistics/morib_kuala_lumpur
https://www.windfinder.com/windstatistics/singapore_changi

Table S2b. Monthly precipitation (mm)

	Jan	Feb	mar	Apr	May	Jun	Jul	Aug	Sep	Oct	Nov	Dec
Philippines	5	34	10	23	126	101	274	648	96	251	44	66
Malaysia	115	110	154	254	427	235	315	149	174	169	629	290
Singapore	293	231	177	260	174	115	137	123	124	228	378	409

Philippines: measurements for Manila, year: 2016; data from www.worldweatheronline.com
Malaysia: measurements for Kuala Lumpur, year: 2016; data from www.worldweatheronline.com
Singapore: measurements for Singapore City, year: 2016; data from www.worldweatheronline.com

Table S3a. ^{210}Pb and ^{137}Cs concentrations in core MOH taken from Mohicap, Philippines.

Depth	Dry Mass	Pb-210						Cs-137	
		Total		Supported		Unsupp			
cm	g cm^{-2}	Bq Kg^{-1}	±	Bq Kg^{-1}	±	Bq Kg^{-1}	±	Bq Kg^{-1}	±
2.0	0.1907	186.45	25.77	41.13	7.19	145.32	26.75	0	0
5.5	0.5337	175.01	20.89	28.81	5.66	146.20	21.64	0	0
11.5	1.3437	191.27	21.59	36.55	6.01	154.72	22.41	0	0
17.5	2.6547	147.99	16.05	37.85	4.40	110.17	16.64	0	0
23.5	4.8498	130.70	15.00	16.56	3.75	114.14	15.46	0	0
29.5	7.6704	75.04	7.55	31.72	2.04	43.32	7.82	0	0
35.5	9.5238	98.93	13.53	29.01	3.68	69.92	14.02	3.31	1.68
41.5	11.2548	101.49	10.56	29.24	2.69	72.25	10.90	0	0
47.5	15.9975	33.67	11.68	38.63	3.69	-4.96	12.25	0	0
54.5	23.5701	59.87	18.72	36.92	2.46	-7.05	18.88	0	0
61.5	29.5457	42.00	23.36	52.03	6.03	-10.03	24.13	0	0

Table S3b. ^{210}Pb and ^{137}Cs concentrations in core SAMP taken from Sampaloc, Philippines.

Depth	Dry Mass	Pb-210						Cs-137	
		Total		Supported		Unsupp			
cm	g cm^{-2}	Bq Kg^{-1}	±	Bq Kg^{-1}	±	Bq Kg^{-1}	±	Bq Kg^{-1}	±
0.5	0.031	189.61	18.76	25.84	3.89	163.77	19.16	0	0
3.5	0.4713	125.17	14.04	27.33	3.37	97.84	14.44	0	0
7.5	0.9571	161.75	13.73	26.41	3.24	135.34	14.11	0	0
9.5	1.2822	118.42	26.54	40.84	6.16	77.58	27.25	0	0
14.5	1.991	85.44	13.66	43.36	3.02	42.08	13.99	0	0
19.5	2.6652	212.88	33.03	51.12	7.85	161.76	33.95	0	0
22.5	3.0848	86.63	13.83	31.69	3.62	54.94	14.3	0	0
25.5	3.5043	112.18	25.03	54.37	6.42	57.81	25.84	0	0
28.5	3.9305	92.49	13.38	33.4	4.36	59.09	14.07	0	0
31.5	4.3566	66.32	13.75	37.64	4.63	28.68	14.51	0	0
35.5	4.9398	41.12	9.37	31.3	3.21	9.82	9.9	0	0
39.5	5.523	61.48	9.88	33.56	3.21	27.92	10.39	0	0
42.5	6.0576	55.44	7.79	30.8	2.47	24.64	8.17	0	0
46.5	6.7704	38.22	9.15	46.47	2.47	-8.25	9.48	0	0
54.5	8.4348	38.22	9.86	38.83	2.48	-0.61	10.17	0	0
69.5	11.7134	25.03	7.75	31.78	2.32	-6.75	8.09	0	0

Table S3c. ^{210}Pb and ^{137}Cs concentrations in core YAMB taken from Yambo, Philippines.

Depth	Dry Mass	Pb-210						Cs-137	
		Total		Supported		Unsupp			
cm	g cm^{-2}	Bq Kg^{-1}	±	Bq Kg^{-1}	±	Bq Kg^{-1}	±	Bq Kg^{-1}	±
0.75	0.1188	210.23	17.38	44.97	4.19	165.26	17.88	0	0
4.5	1.0329	173.6	13.81	38.15	3.17	135.45	14.17	4.29	1.33
9.5	1.9378	159.12	18.7	43.17	4.14	115.95	19.15	0	0
12.5	2.446	115.47	12.66	36.25	3.18	79.22	13.05	0	0
14.5	2.7848	102.58	12.45	37.75	3.39	64.83	12.9	0	0
17.5	3.341	112.62	13	28.15	2.98	84.47	13.34	0	0
19.5	3.7118	149.55	13.55	48.8	3.7	100.75	14.05	0	0
25.5	5.2979	94.3	8.33	44.43	2.13	49.87	8.6	5.21	0.79
27.5	5.8124	73.8	10.19	35.54	2.75	38.26	10.55	0	0
31.5	6.8414	78.78	11.31	38.36	3.21	40.42	11.76	6.43	1.47
33.5	7.2229	62.26	6.77	31.53	1.78	30.73	7	6.34	0.85

36.5	7.7952	81	11.4	45.26	2.99	35.74	11.79	6.12	1.4
39.5	8.3674	81.38	8.27	41.49	2.18	39.89	8.55	15.94	1.23
46.5	9.507	69.45	10.09	38.75	2.81	30.7	10.47	0	0
54.5	10.787	27.21	6.82	39.71	2.03	-12.5	7.12	1.53	0.82
61.5	12.0589	42.3	8.39	43.69	2.97	-1.39	8.9	2.86	1.37
69.5	13.3613	48.04	7.33	36.11	2.57	11.93	7.77	0	0
79.5	16.7343	27.91	4.81	34.25	1.59	-6.34	5.07	0	0

Table S3d. ^{210}Pb and ^{137}Cs concentrations in core TC-1a taken from Tasik Chini, Malaysia

Depth	Dry Mass	Pb-210						Cs-137	
		Total		Supported		Unsupp			
cm	g cm^{-2}	Bq Kg^{-1}	±	Bq Kg^{-1}	±	Bq Kg^{-1}	±	Bq Kg^{-1}	±
0.5	0.0629	222.37	18.68	99.3	6.6	123.07	19.81	0	0
3.5	0.5566	261.24	25.25	101.91	6.87	159.33	26.17	0	0
6.5	1.3096	258.91	15.12	93.59	4.21	165.32	15.7	0	0
9.5	2.0703	180.6	12.69	103.94	4.13	76.66	13.35	0	0
12.5	2.831	289.54	17.23	121.56	5.16	167.98	17.99	0	0
15.5	3.4948	243.46	14.61	127.83	4.59	115.63	15.31	0	0
18.5	4.1993	246.71	8.2	130.11	2.51	116.6	8.58	1.70	0.93
20.5	4.727	231.31	14.74	125.17	4.66	106.14	15.46	0	0
21.5	4.9952	222.06	13.18	138.56	4.66	83.5	13.98	3.21	1.61
24.5	5.8104	207.79	14.69	149.46	4.85	58.33	15.47	0	0
27.5	6.6602	208.11	14.27	146.57	4.81	61.54	15.06	0	0
29.5	7.242	193.97	12.92	130.19	4.32	63.78	13.62	0	0
30.5	7.5406	168	8.22	133.3	2.64	34.7	8.63	0	0
31.5	7.867	175.94	12.34	131.88	4.09	44.06	13	0	0
33.5	8.47	163.96	12.98	131.15	4.36	32.81	13.69	0	0
36.5	9.1938	229.49	18.23	147.58	5.82	81.91	19.14	0	0
39.5	9.8468	204.35	10.35	151.23	3.57	53.12	10.95	0	0
42.5	10.4958	169.54	13.99	147.42	4.96	22.12	14.84	0	0
45.5	11.174	139.73	12.95	143.78	4.8	-4.05	13.81	0	0
48.5	11.8296	147.14	16.61	143.79	4.74	3.35	17.27	0	0

Figure S1a: Typical plot of variations over time in altitude of air parcels arriving at three study sites: January 1st 2017

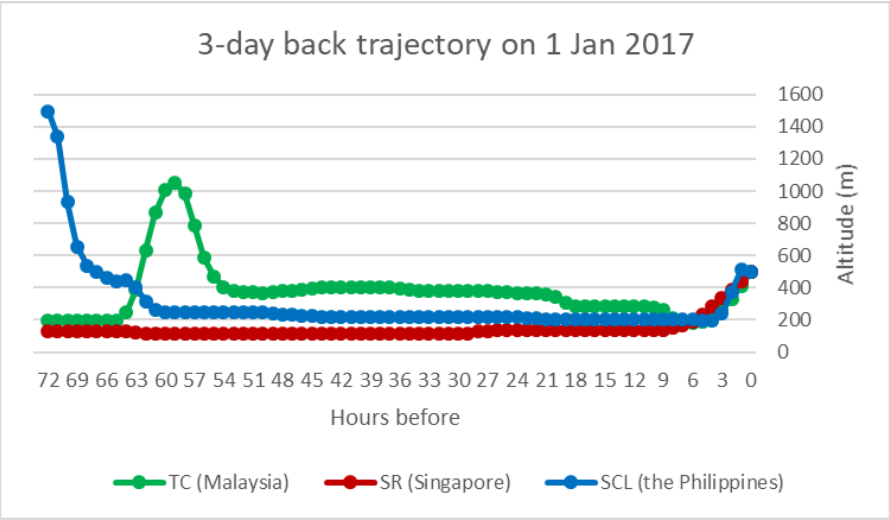

Figure S1b: Typical plot of variations over time in altitude of air parcels arriving at three study sites: May 1st 2016

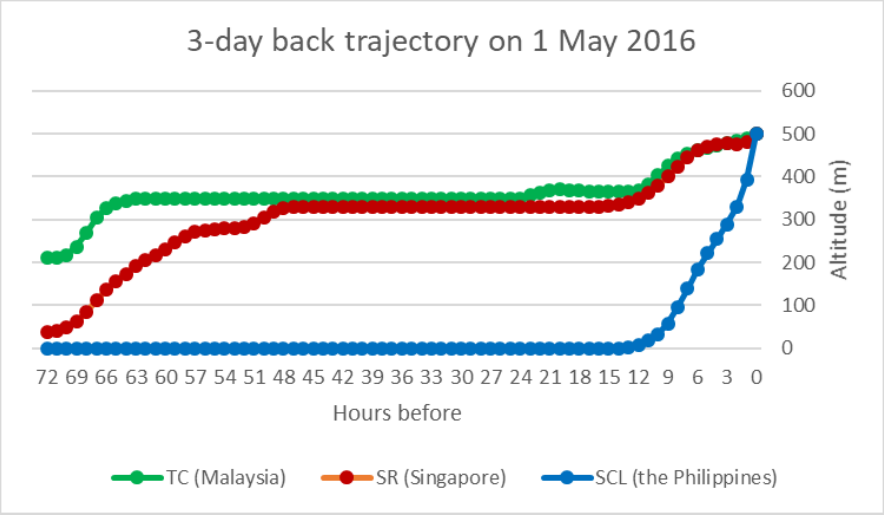

Figure S1c: Typical plot of variations over time in altitude of air parcels arriving at three study sites: August 1st 2016

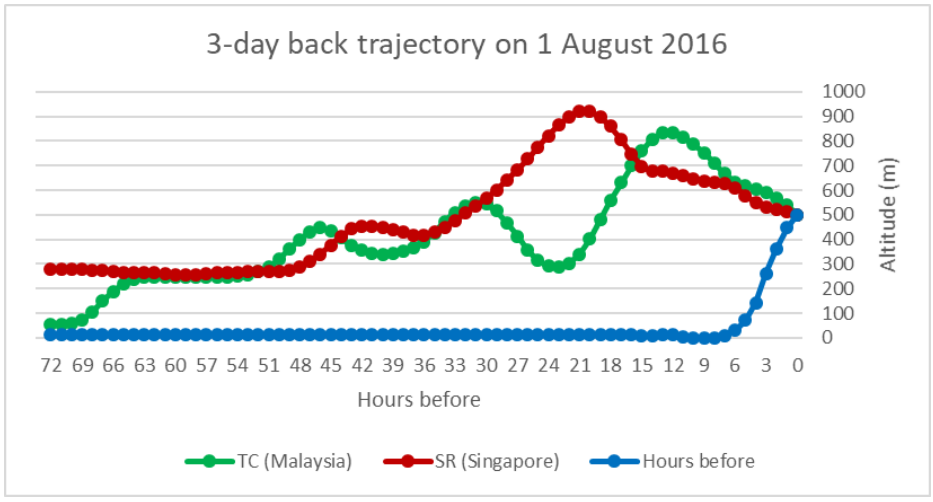

Figure S1d: Typical plot of variations over time in altitude of air parcels arriving at three study sites: October 1st 2016

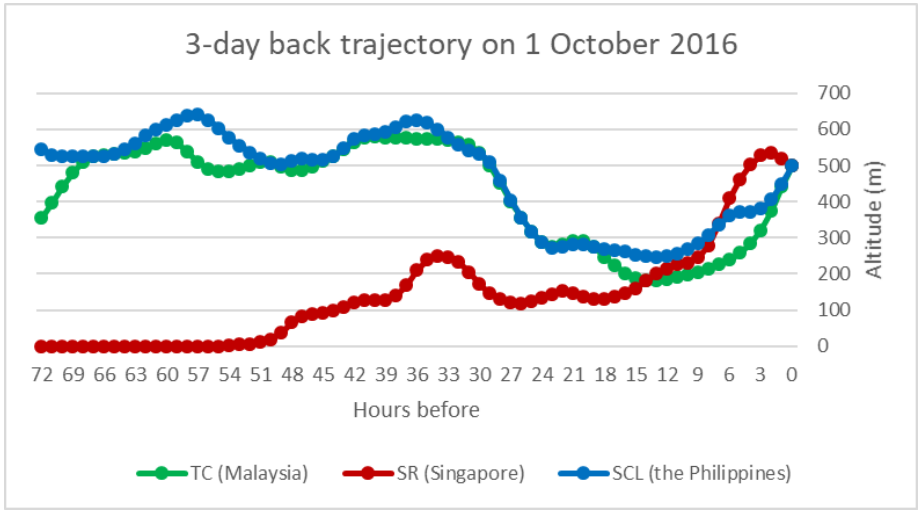

Figure S1e: Typical plot of variations over time in altitude of air parcels arriving at three study sites: November 1st 2016